Article:
Jones, R, Thomas, RE, Peakall, J et al. (1 more author) (2017) Rainfall-runoff properties of tephra: Simulated effects of grain-size and antecedent rainfall. Geomorphology, 282. pp. 39-51. ISSN 0169-555X

https://doi.org/10.1016/j.geomorph.2016.12.023

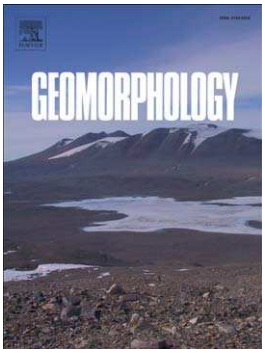

Rainfall-runoff properties of tephra: Simulated effects of grain-size and antecedent rainfall

Robbie Jones, Robert E. Thomas, Jeff Peakall, Vern Manville

PII: S0169-555X(16)30600-6
DOI: doi:10.1016/j.geomorph.2016.12.023
Reference: GEOMOR 5869

To appear in: *Geomorphology*

Received date: 12 July 2016
Revised date: 23 December 2016
Accepted date: 23 December 2016

Please cite this article as: Jones, Robbie, Thomas, Robert E., Peakall, Jeff, Manville, Vern, Rainfall-runoff properties of tephra: Simulated effects of grain-size and antecedent rainfall, *Geomorphology* (2017), doi:10.1016/j.geomorph.2016.12.023

Rainfall-runoff properties of tephra: Simulated effects of grain-size and antecedent rainfall

Robbie Jones*, Robert E. Thomas, Jeff Peakall, Vern Manville

School of Earth and Environment, University of Leeds, Leeds, LS2 9JT, UK

*Corresponding author.

Tel: +447875840776; Fax: +44 113 343 5259

E-mail address: eerj@leeds.ac.uk (R. Jones)

Abstract

Rain-triggered lahars (RTLs) are a significant and often persistent secondary volcanic hazard at many volcanoes around the world. Rainfall on unconsolidated volcaniclastic material is the primary initiation mechanism of RTLs: the resultant flows have the potential for large runout distances (>100 km) and present a substantial hazard to downstream infrastructure and communities. RTLs are frequently anticipated in the aftermath of eruptions, but the pattern, timing and scale of lahars varies on an eruption-by-eruption and even catchment-by-catchment basis. This variability is driven by a set of local factors including the grain size distribution, thickness, stratigraphy and spatial distribution of source material in addition to topography, vegetation coverage and rainfall conditions. These factors are often qualitatively discussed in RTL studies based on post-eruption lahar observations or instrumental detections. Conversely, this study aims to move towards a quantitative assessment of RTL hazard in order to facilitate RTL predictions and forecasts based on constrained rainfall, grain size distribution and isopach data. Calibrated simulated rainfall and laboratory-constructed tephra beds are used within a repeatable experimental set-up to isolate the effects of individual parameters and to examine runoff and infiltration processes from analogous RTL source conditions.

Laboratory experiments show that increased antecedent rainfall and finer-grained surface tephra individually increase runoff rates and decrease runoff lag times, while a combination of these factors produces a compound effect. These impacts are driven by increased residual moisture content and decreased permeability due to surface sealing, and have previously been inferred from downstream observations of lahars but not identified at source. Water and sediment transport mechanisms differ based on surface grain size distribution: a fine-grained surface layer displayed airborne remobilisation, accretionary pellet formation, rapid surface sealing and infiltration-excess overland flow generation whilst a coarse surface layer demonstrated exclusively rainsplash-driven particle detachment throughout the rainfall simulations. This experimental protocol has the potential to quantitatively examine the effects of a variety of individual parameters in RTL initiation under controlled conditions.

Keywords: Rain-triggered Lahars; Rainfall Simulation; Tephra; Runoff

1. Introduction

Rainfall on unconsolidated volcaniclastic material, typically pyroclastic density current (PDC) and/or ash-fall deposits, is the primary initiation mechanism of secondary, rain-triggered lahars (RTLs). These flows pose a significant hazard to downstream infrastructure, with impacts ranging from damage to building contents via flow inundation, to complete destruction and burial of structures (Jenkins et al., 2015). RTLs often pose a long-lived secondary hazard, with discrete large eruptions resulting in significant catchment disturbance for many decades (Major et al., 2000; Gran and Montgomery, 2005; Major and Yamakoshi, 2005; Van Westen and Daag, 2005; Major and Mark, 2006). The combination of intense rainfall and a source of volcaniclastic material required for RTL initiation is particularly common throughout the tropics and sub-tropics, and has been documented at volcanoes including Mayon (Arguden and Rodolfo, 1990; Rodolfo and Arguden, 1991; Orense and Ikeda, 2007; Paguican et al., 2009), Pinatubo (Arboleda and Martinez, 1996; Martinez et al., 1996;

Rodolfo et al., 1996; Tungol and Regalado, 1996; Van Westen and Daag, 2005), Merapi (Lavigne et al., 2000a,b; Lavigne and Thouret, 2003; de Bélizal et al., 2013), Semeru (Lavigne and Suwa, 2004; Doyle et al., 2010; Dumaisnil et al., 2010; Thouret et al., 2014), Soufriere Hills (Barclay et al., 2007), Colima (Davila et al., 2007; Capra et al., 2010) and Tungurahua (Jones et al., 2015), illustrating the global extent of locations with significant documented histories of RTL activity.

The initiation of RTLs typically occurs via either particle detachment by rainsplash erosion and subsequent transport by overland flow (Segerstrom, 1950; Waldron, 1967), rill erosion caused by surface runoff (Nammah et al., 1986; Leavesley et al., 1989; Yamakoshi and Suwa, 2000; Lavigne and Thouret, 2003; Major and Yamakoshi, 2005; Barclay et al., 2007) or by shallow landsliding of saturated tephra layers above basal décollement surfaces (Rodolfo and Arguden, 1991; Hodgson and Manville, 1999; Manville et al., 2000; Jensen et al., 2013) (Fig. 1). Numerous temporally and spatially variable factors contribute towards these lahar initiation processes including grain size distribution (Pierson et al., 2013), thickness (Janda et al., 1996; Scott et al., 1996; Manville et al., 2000), extent of compaction (Manville et al., 2000) and volatile content (Waldron, 1967) of pyroclastic material; vegetation cover (Yamakoshi and Suwa, 2000; Barclay et al., 2007; Ogawa et al., 2007; Alexander et al., 2010) and type (Capra et al., 2010); rainfall intensity and duration (Rodolfo and Arguden, 1991; Lavigne et al., 2000b; Van Westen and Daag, 2005; Hikida et al., 2007; Okano et al., 2012); slope angle (Pierson et al., 2013) and antecedent rainfall (Lavigne et al., 2000b; Barclay et al., 2007; Okano et al., 2012; Jones et al., 2015) (Fig. 2).

The deposition mechanism of the volcaniclastic material, usually either PDC or ash-fall deposits, plays an important role in controlling spatio-temporal variability of RTL initiation. PDC deposits typically contain more fines as a result of a lack of aerodynamic sorting, are generally valley confined, and usually eroded by headward migration of knickpoints and channel widening/bank collapse (Manville et al., 2009; Pierson and Major, 2014). Ash-fall deposits mantle the topography, are thinner, more widely distributed, better sorted, and easily eroded by rilling, uniform sheetwash

or shallow landsliding (Pierson and Major, 2014). They typically display an exponential decrease in particle size and deposit thickness with increased distance from the vent but dispersal patterns can be more complex (e.g. Brazier et al., 1983). The surface of ash-fall deposits often undergoes post-deposition surface sealing and crusting as a result of raindrop impact and/or chemical precipitation, a process which increases surface resistance to erosion but also increases runoff (Waldron, 1967). Once the surface crust has been disturbed, runoff can remobilise underlying material, potentially resulting in RTL initiation (Waldron, 1967). PDC deposits are described by Pierson and Major (2014) as loose and highly erodible by rainfall and streamflow; although large, hot PDCs can produce deposits featuring welded zones which are more resistant to erosion. Ash-fall can damage vegetation via abrasion, weight-induced failure, burial, chemical damage or interference with leaf surface metabolic activity (Alexander et al., 2010; Swanson et al., 2013; Pierson and Major, 2014). PDCs can sand blast, burn, fell and in some examples strip and remove all vegetation within a valley (Pierson, 1985; Pierson and Major, 2014; Stinton et al., 2014).

Rainfall intensity/duration relationships have been a frequently utilised method of post-eruption RTL analysis. Studies at volcanoes including Pinatubo (Arboleda and Martinez, 1996; Tungol and Regalado, 1996; Van Westen and Daag, 2005), Mayon (Rodolfo and Arguden, 1991), Tungurahua (Jones et al., 2015), Merapi (Lavigne et al., 2000b) and Colima (Capra et al., 2010) have used this method, which typically displays a power-law relationship that suggests that lahar initiation occurs along a continuum from short duration, high intensity rainfall events to long duration, low-intensity events. Intensity/duration analysis compiles datasets of identified and/or instrumentally-detected lahars and identifies the range of rainfall conditions under which lahars can potentially occur. Probabilistic analysis and forecasting of lahars has been undertaken at Tungurahua (Jones et al., 2015) using peak rainfall intensity and antecedent rainfall data. Probabilistic analysis of this nature uses the lahar and rainfall databases to examine the likelihood of lahars under different rainfall conditions and then applies it to real-time rainfall data to make lahar forecasts. Probabilistic lahar forecasting acknowledges the uncertainty present in the lahar triggering rainfall range identified

during intensity/duration analysis. Such uncertainty is difficult to constrain during field-based studies due to the challenges of observing lahar initiation zones, given their typical proximity to the active vents of frequently eruptive volcanoes. This access issue, in combination with the complex nature of RTL initiation processes, makes it difficult to isolate the impacts of individual parameters upon RTL initiation. Rainfall simulation experiments are one method of approaching this issue, and have previously been utilised to study rainfall-runoff relationships in other disturbed earth systems such as wildfire-affected areas. Such simulations have typically been either field-based (e.g. Pierson et al., 2008; Woods and Balfour, 2010; Huang et al., 2013; Zhao et al., 2014) or lab-based (e.g. Bradford et al., 1987; Singh et al., 2000; Jomaa et al., 2013; Wang et al., 2014) and have focused on a variety of parameters using different slope angles, rainfall regimes and bed compositions (Römkens et al., 2002; Liu et al., 2011; Huang et al., 2013).

Previous rainfall simulation studies have indicated that enhanced vegetation cover, and thus the process of vegetation recovery, increases infiltration and decreases runoff and erosion rates. This is a result of heightened permeability due to surface seal and crust disruption as well as increased soil stability and rainfall interception (Morgan et al., 1997; Major and Yamakoshi, 2005; Cerda and Doerr, 2008; Huang et al., 2013; Zhao et al., 2014). Elevated slope angle and rainfall intensity increase runoff rates due to heightened occurrence of infiltration-excess overland flow (Horton, 1933; Luk, 1985; Liu et al., 2011; Huang et al., 2013; Jomaa et al., 2013). High surface moisture content and thus surface water potential, often induced by significant antecedent rainfall or long-duration rainfall events, acts to increase rainsplash-driven particle detachment in inter-rill regions via a reduction in surface shear strength (Luk, 1985; Bryan, 2000). In addition, increased surface roughness was shown by Römkens et al. (2002) to increase sediment yield under pre-defined rainfall conditions and rill development is heightened on steeper slopes (Gómez et al., 2003). Zhao et al. (2014) described runoff mechanisms on grassland plots under rainfall simulation conditions as infiltration-excess overland flow-dominant regardless of antecedent conditions, with saturation-excess flow occurring simultaneously after rainfall of sufficient duration. Despite such examples,

quantitative studies of the relationship between rainfall intensity, antecedent conditions and surface sealing (important factors in RTL initiation) are limited (Jomaa et al., 2013), and while the systems studied to date have some parallels with elements of RTL initiation environments, none have focused specifically on RTLs. This study aims to use calibrated rainfall simulations to identify the impact of grain size distribution and antecedent rainfall upon the rainfall-runoff properties of fresh tephra deposits in conditions analogous to those present in RTL initiation zones.

2. Methods

2.1. Ash bed

Two airfall tephra samples were used during this study. The first was produced by the plinian andesitic eruption of Mt. Kelud, Indonesia on 13th February 2014. The second sample was a product of the plinian rhyolitic eruption of Chaitén, Chile in 2008. Both of these eruptions generated a RTL hazard due to the widespread deposition of pyroclastic sediments (Pierson et al., 2013; Umazano et al., 2014; Dibyosaputro et al., 2015; Major et al., 2016). The Chaitén sample was finer (D_{50} = 54.3 µm) than the Kelud sample (D_{50} = 525.8 µm) (Table 1; Fig. 3), offering a contrast in simulated lahar initiation conditions.

Ash bed construction was dictated by the requirement to constrain the bulk density of the tephra while maintaining an experimental set-up which replicated natural conditions. To achieve this, ash beds were constructed within a 0.3×0.3×0.1 m stainless steel insert inside a rigid 0.3×0.3 m shear box. Ash beds were lightly compacted using a 0.3×0.3 m 10 kg mass, which was applied under gravity for 1800 s. The use of a shear box in this manner ensured that all samples were compacted under consistent normal and lateral stresses and rates of strain, while preventing the application of any shear. This approach also ensured no deformation of the walls of the ash bed during construction, thus allowing accurate capture of the mass and volume of tephra.

Samples were air dried, resulting in initial moisture contents by weight of 0.05% (Kelud) and 0.11% (Chaitén). Two types of ash bed were constructed: Ash Bed 1 (AB1), which consisted purely of the coarse Kelud ash (0.1 m depth) and Ash Bed 2 (AB2), which comprised 0.095 m depth of Kelud ash topped with 5 mm of finer Chaitén ash. These proportions were driven primarily by the availability of the different samples. The beds were each constructed in three uniform layers, with light raking of the surface of lower layers to minimise discontinuities (Huang et al., 2013). The surface was finally smoothed, levelled and lightly compacted, resulting in similar bulk densities of 1468 kg m^{-3} (AB1) and 1467 kg m^{-3} (AB2). These bulk tephra densities are within the range of 1200–1600 kg m^{-3} reported by Spence et al. (2005) from the eruption of Mt. Pinatubo in 1991 and close to the 1400 and 1450 kg m^{-3} values described at Eyjafjallajökull (Gudmundsson et al., 2012) and Pillate, Tungurahua (Bernard, 2013), respectively. When completed, the ash beds and steel insert were removed from the shear box and placed in a 75 mm-deep plastic tray on top of a micro-porous steel mesh. The base of the tray was free-draining to allow water to pass through the bottom of the ash bed.

2.2. *Rainfall simulator*

A rainfall simulator was designed and constructed to replicate lahar-triggering rainfall under laboratory conditions. The experimental configuration (Fig. 4) consisted of a water tank, pulse-free gear pump, flow meter and nozzle-holding frame. The nozzles (Fulljet-1/2HH-30WSQ and Fulljet-1/2HH-40WSQ) were held by the frame at a height of 2.3 m above the ground, the maximum possible ground clearance. In order to determine the optimal configuration for the production of analogous rainfall, and to identify the optimal sub-area within the 1 m^2 calibration area in which to locate the 0.3×0.3 m ash bed, calibration of the rainfall rate was performed across a surface area of 1 m^2 using 65 spatially-distributed rainfall collection vessels, each with a diameter of 30 mm (Loch et al., 2001). During each calibration experiment, the rainfall simulator was run for a period of 60 s and

then the mass of water was measured in each container. Different pump settings (and therefore flow rates) were tested, with each nozzle separately tested for each pump setting and each pump setting/nozzle combination repeated three times. Simulator performance was assessed both in terms of rainfall intensity and uniformity. Uniformity was quantified using Christiansen's uniformity coefficient (C_u; Christiansen, 1942). This coefficient takes as parameters the mean value ($\bar{x}$), the number of observations (n) and the sum of the deviations from the mean: $\sum_1^n(x-\bar{x})$. It is expressed as a percentage; a higher percentage indicating more uniform rainfall, with values over 80% considered sufficient for successful rainfall simulations (Loch et al., 2001).

$$C_u = 100\left(1 - \frac{\sum_1^n(x-\bar{x})}{n\bar{x}}\right) \quad (1)$$

The selected configuration produced a flow rate of 8×10^{-4} m^3 s^{-1}. The spatial distribution of rainfall intensity produced by this configuration across both the entire 1 m^2 rainfall calibration area and the optimal 0.3×0.3 m ash bed location is shown in Fig. 5. The mean rainfall intensity for the entire rainfall calibration area under the rainfall conditions shown in Fig. 5 was 2.5 mm min^{-1} with a C_u value of 79.1%, but this value was improved in the optimal 0.3×0.3 m sub-plot to 1.7 mm min^{-1} with a C_u value of 91.9%. This rainfall intensity represents intense lahar-triggering rainfall; for example, it would be expected to trigger a lahar 100% of the time if sustained for >600 s at Tungurahua using the forecasting approach of Jones et al. (2015). Similar sustained rainfall intensity values are documented in many tropical rainfall datasets including Larsen and Simon (1993), Van Westen and Daag (2005) and Thouret et al. (2014).

2.3. *Experiment configuration*

Fig. 4 illustrates the experimental configuration, featuring both the ash bed and rainfall simulator components. The ash bed was fitted onto a frame providing an angle of 28.2°, which was kept constant during this study. The use of this frame provided a minimum nozzle height of 1.91 m

above the upslope extremity of the ash bed surface. A gutter hopper was fitted at the downslope edge of the ash bed in order to funnel surface runoff into a beaker atop a mass balance (Ohaus NV4101; 0.2 g resolution), generating a continuous time series of runoff volume. Underneath the ash bed, a tray of identical dimensions sat atop a second mass balance, generating a continuous time series of infiltrated rainfall as it passed through the base of the 0.1 m-thick ash bed. A skirt around the sides of the frame waterproofed the infiltration tray and runoff beaker while a shield was in place to prevent rainfall directly entering the runoff gutter. High definition video cameras capturing 30 frames per second recorded continuous video of both the mass balance screens and the surface of the ash bed (Fig. 4).

Rainfall simulations were 1200 s in duration and were predominantly separated by consecutive “dry” periods of 24 hours. AB1 was used for four simulations (1.1–1.4), each separated by 24 hours. AB2 featured five simulations, the first four also separated by 24 hours (2.1–2.4) and the last (2.5) after an extended “dry” period of 120 hours. This method generated a range of pre-simulation antecedent conditions (Table 2), with the magnitude of 72-hour antecedent rainfall ranging from a minimum of 0 mm (Simulations 1.1, 2.1 and 2.5) to a maximum of 102 mm (Simulations 1.4 and 2.4). Time series of both runoff and infiltration through the base of the ash bed were recorded, as was footage of surface processes during the simulation.

Moisture content was analysed by oven drying samples before the first and immediately after the last simulation of each ash bed. The former used tephra samples from which the ash beds were constructed, while the latter was achieved by taking cores from the ash beds immediately after the final simulations. Samples were subsequently oven dried at 50°C until intermittent recordings of mass ceased to decrease. Moisture content could not be calculated after each individual simulation as disturbance of the ash bed surface would impact runoff and erosion in subsequent rainfall simulations.

3. Analysis

3.1. *Surface processes*

The first rainfall simulations of each ash bed (1.1 and 2.1) demonstrate the behaviour of dry tephra deposits when initially exposed to rainfall. Video footage of the surfaces of AB1 and AB2 illustrates contrasting processes under such conditions, driven by the difference in grain size distribution at the surface (Fig. 6). The development of AB1 during simulation 1.1 is shown in Fig. 6A–C. The behaviour of this coarse ash bed was characterised by a darkening in colour once rainfall was applied, an absence of visible surface runoff generation and a lack of surface texture variation. Particle movement was dominated by rainsplash-driven detachment of individual coarse tephra grains, with no obvious rill formation or overland flow. As can be seen in Fig. 6A–C there was little visual change in the surface texture of AB1 during the first 870 s of simulation 1.1. Individual coarse particles reached the AB1 runoff collection vessel via particle detachment, but at low frequency. AB1 displayed little visual change during simulations 1.2–1.4, with rainsplash particle detachment remaining the dominant re-mobilisation mechanism. In contrast, the fine-grained surface layer of AB2 underwent significant visual change during the course of simulation 2.1 (Fig. 6D–I). With the onset of rainfall, the initial smooth, off-white surface immediately changed due to a combination of particle detachment and ash pellet formation. Particle detachment produced visible “puffs” of airborne ash upon raindrop impact as opposed to the visible parabolic movement of individual particles during simulation 1.1. Pellets of ash formed as raindrops impacted the dry surface ash, with some ash pellets subsequently rolling downslope (Fig. 6E). These processes continued throughout the first 60 s of simulation 2.1, with visible particle detachment and pellet formation decreasing with time as the entire surface wetted up. Pellets of ash led to a rough, undulating surface across AB2 (Fig. 6F), similar to the “curd texture” identified at Mt. Ruapehu by Manville et al. (2000). The first signs of surface runoff as Hortonian infiltration-excess overland flow, a product of surface sealing due to raindrop impact, occurred after 95 s and this soon became the dominant process of tephra re-mobilisation. Fig. 6G–H illustrate the inundation of the entire rough surface of AB2 with

Hortonian overland flow within 240 s of the start of the simulation. Over the remaining 960 s, overland flow was the dominant mechanism driving sediment transport and, together with physical raindrop impact, smoothed the surface of AB2 (Fig. 6I). Overland flow continued to be the dominant mechanism of sediment transport throughout simulations 2.2–2.4, resulting in the deposition of entrained fine-grained material in the runoff collection vessel. Nevertheless, it was noted that the erosion of AB2 during simulations 2.1–2.5 was not sufficient to visually expose the underlying coarse, more permeable tephra.

3.2. *Rainfall and runoff*

Both total runoff volumes and runoff-rates (Fig. 7) increased from simulations 1.1–1.4 and 2.1–2.4; i.e. with increased antecedent rainfall (Table 2). Runoff rates from AB1 were lower than AB2, with simulations 2.3 and 2.4 producing runoff rates over an order of magnitude higher than simulations 1.3 and 1.4 under identical antecedent conditions. Initial impacts of an extended dry period (120 hours) can be seen in the total runoff values produced during simulation 2.5, which were 80% lower than the preceding simulation (2.4) and less than those produced during simulation 2.1 (Fig. 7). Runoff sediment concentration was negligible for AB1 simulations, with isolated coarse grains re-mobilised by rainsplash-driven particle detachment the only sediment to reach the runoff beaker. The sediment concentration of AB2 runoff was higher due to surface runoff entrainment but still low due to the lack of rill erosion within the rainfall simulations as a result of the limited slope length of the ash bed. AB2 mean runoff sediment concentrations (by weight) increased from 0.42% (2.1) to 0.60% (2.2) and reached a peak sediment concentration of 1.16% (2.3). Subsequent simulations (2.4 & 2.5) produced mean sediment concentrations of approximately 1% and 1.05%, respectively. The recorded runoff sediment mass from each AB2 simulation indicates that cumulative erosion resulted in the removal of at least 5.2% of the fine-grained surface layer of AB2

at the end of simulation 2.5. Maximum erosion from an individual simulation occurred during simulation 2.4 (2.1%).

In addition to the absolute increase in AB2 runoff rate compared with AB1 (Fig. 7), the impact of antecedent rainfall upon runoff relative to the initial simulations was enhanced for AB2 (Fig. 8). This is further emphasised in Fig. 9, which isolates the final runoff totals at the end of AB1 and AB2 simulations and displays both the higher total runoff from AB2 compared to AB1 and the greater rate of AB2 runoff increase with heightened antecedent rainfall. When considering the total 1200 s runoff, both AB1 and AB2 exhibited increased runoff with increased antecedent rainfall. However, runoff increased by 292% for simulation 2.4 relative to 2.1 while this increase was only 18% for 1.4 relative to 1.1 (Fig. 8). Individual simulation-by-simulation increases in total runoff for AB2 simulations were 79% (2.1–2.2), 60% (2.2–2.3) and 38% (2.3–2.4). When the simulations are divided into four sub-periods of 300 s, it can be seen that the most marked impact of increased antecedent rainfall on runoff occurred during the first 300 s (Figs. 8 and 10). Runoff during this initial 300 s sub-period increased by 553% for simulation 2.4 relative to 2.1 and 334% for simulation 1.4 relative to 1.1 (Fig. 8B). Comparing simulation 2.4 to simulation 2.1, runoff increased by >200% in each of the four 300 s duration sub-periods (Fig. 8B). Conversely, comparing simulation 1.4 to simulation 1.1, runoff increased by only 44% for the 300–600 s sub period and decreased by approximately 20% during each of the last two 300 s duration sub-periods (Fig. 8A).

Despite the biggest antecedent rainfall-driven impact on runoff rates occurring in the first 300 s of a rainfall simulation, runoff rates predominantly increase with time during simulations (Fig. 10). This increase during the simulation is largest and most consistent under conditions of low antecedent rainfall. As antecedent rainfall increased, runoff rates for the 300 s sub-periods converged, resulting in less extreme runoff rate increases during the simulations.

Variations in runoff rates between AB1 and AB2 impact runoff lag time, which in this study is defined as the time period between the beginning of the rainfall simulation and the recording of 10

g of surface runoff. In both simulations, lag times declined as antecedent rainfall was increased (Fig. 11). Lag times were higher for AB1 than AB2 because of the coarse nature of the ash bed and the dominant mechanism of downslope transport: rainsplash and particle detachment.

Examining the temporal change in the relationship between runoff and infiltration during each rainfall simulation provides insight into the destination of applied rainfall under different conditions. Apparent infiltration rates (f') (Hawkins and Cundy, 1987; Dunne et al., 1991; Yu et al., 1997) during each of the rainfall simulations are derived using the average plot-scale rainfall rate (I) and recorded runoff rate (q).

$$f' = I - q \qquad (2)$$

Previous studies have identified that apparent infiltration rates measured both in the field and in laboratory-based rainfall simulator experiments vary with slope angle and rainfall intensity (Hawkins and Cundy, 1987; Dunne et al., 1991; Major and Yamakoshi, 2005). In the present study, rainfall intensity and slope angle are constant, facilitating the inter-simulation comparison of apparent infiltration rates across all AB1 and AB2 simulations (Fig. 12). AB1 simulations displayed consistently high rates of apparent infiltration, with a small linear decrease in apparent infiltration rates with time during the simulations (Fig. 12). All AB2 simulations displayed decreased apparent infiltration rates relative to AB1 simulations (Fig. 12), with the apparent infiltration rates of AB2 demonstrating exponential decay during the rainfall simulations (Fig. 12). Apparent infiltration rates progressively decreased during simulations 2.1–2.4, but simulation 2.5 displayed the highest apparent infiltration rates of all AB2 simulations, illustrating the impact of an extended dry period of 120 hours.

Moisture content ($mass_{water}/mass_{ash+water}$) was calculated for tephra samples (Kelud and Chaitén) prior to ash bed construction and for both AB1 and AB2 immediately after the last simulations (1.4 and 2.5, respectively). Moisture content for the “dry” Kelud sample was 0.05%, while the moisture content for the “dry” Chaitén sample was 0.11%. The moisture content of the

AB1 ash bed was 17.39% immediately after simulation 1.4, while that of the AB2 ash bed was 17.11% immediately after simulation 2.5.

4. Discussion

4.1. Grain size distribution

Variation in the grain size distribution of pyroclastic material is one of the primary factors impacting the frequency and mechanism of RTL initiation (e.g. Manville et al., 2000; Pierson et al., 2013). Runoff increased by up to 1500% for AB2 compared to AB1 under identical antecedent conditions (Fig. 9), a product of the reduced permeability of the fine-grained surface layer of AB2. Runoff rates were further enhanced by surface sealing in AB2, which occurs as a product of aggregate breakdown, rearrangement of disrupted fragments, compaction and flattening (Slattery and Bryan, 1992). This surface sealing resulted in decreased infiltration rates and increased resistance to raindrop impact (Bradford et al., 1987). Surface seal development during simulation 2.1, after initial rainsplash-driven particle detachment and the formation of ash pellets, is evident in Fig. 6, with gradual development resulting in widespread overland flow seal 740 s (Fig. 6I) after the onset of rainfall. Increasing runoff rates from simulations 2.1–2.4 indicate that no reduction in surface seal efficiency occurred until the extended dry period prior to simulation 2.5. Owing to the coarse nature of the tephra, such surface sealing did not occur during simulation AB1; infiltration rates were sufficiently high that infiltration-excess overland flow did not occur and raindrop impact resulted in rainsplash-driven particle detachment throughout the simulations. As a result of these surface grain size distribution-driven impacts, apparent infiltration rates (Fig. 12) were lower for all AB2 simulations than AB1 simulations. This highlights the increased potential for lahar initiation as a result of enhanced runoff due to surface sealing of fine-grained surface layers.

The fine-grained surface layer of AB2 also acted to reduce the runoff lag time at the start of the simulations relative to AB1 (in the present study, runoff lag time is defined as the time taken to

record 10 g of runoff). This reduction in lag time was caused by the generation of infiltration-excess overland flow. Due to the limited slope length within the experimental set up, overland flow did not reach sufficient depths or velocities to induce rill erosion. Rills form following the exceedance of the threshold critical fluid shear stress or unit stream power for surface sediment entrainment (Nearing et al., 1989; Gilley et al., 1993). Fluid shear stress is a function of the flow depth and slope angle, while unit stream power is a function of flow depth, velocity and slope angle; for non-cohesive substrata, particle size, shape and mass density control the threshold value required to initiate rilling for a given slope angle (Gilley et al., 1993). Flow rates were not sufficient to induce rill erosion within the present study, but enhanced overland flow in AB2 simulations indicates the potential for rill network development if slope length was increased. Overland flow was minimal during AB1 simulations, which instead relied on rainsplash as the primary mechanism of downslope transport and runoff collection as a result of high infiltration rates (Figs. 11 & 12). The infiltration-dominated regime of AB1 indicates that RTL would require either extreme rainfall intensities or landsliding of the tephra layer above a basal décollement surface when saturated (Manville et al., 2000; Jensen et al., 2013), particularly if emplaced above a less permeable substrate and on a steep slope.

4.2. *Antecedent rainfall*

Increased antecedent rainfall and thus increased moisture content has been shown to enhance surface runoff in a variety of environments (e.g. Tisdall, 1951; Luk, 1985; Le Bissonnais et al., 1995; Castillo et al., 2003). With respect to volcanoes, increased antecedent rainfall has been shown to increase lahar frequency under specific rainfall conditions at locations including Soufrière Hills (Barclay et al., 2007) and Tungurahua (Jones et al., 2015). Rainfall simulations confirm that increased antecedent rainfall (Table 2) acts to increase runoff (Fig. 9), but AB2 displayed a much greater antecedent rainfall-driven impact than AB1. Total runoff from AB1 increased by 18% from simulations 1.1 to 1.4, while this increase was 292% for AB2 from simulations 2.1 to 2.4. The

heightened runoff increase seen in AB2 relative to AB1 illustrates the compound impact of a reduction in pore space between ash particles, an increase in residual tephra moisture content due to prior simulations and enhanced surface sealing of the fine-grained surface layer of AB2. In the absence of surface sealing or infiltration-excess overland flow, the increase in runoff from AB1 is singularly a product of heightened rainsplash as a result of increased surface water content. Demonstrated antecedent rainfall-induced increases in runoff indicate that the peak rainfall intensity required for lahar initiation can be reduced under high antecedent rainfall conditions, an effect that is enhanced when fine-grained surface seal-forming layers are present.

Increased antecedent rainfall also acts to decrease runoff lag times from both AB1 and AB2 (Fig. 11). For AB1, this was a product of enhanced initial rainsplash due to increased residual surface water content. For AB2, this was driven by a reduction of infiltration rate as a product of both increased surface sealing and heightened initial tephra moisture content. Antecedent rainfall-induced lag time reduction suggests that shorter duration rainfall events can still trigger lahars when residual moisture content is high, particularly if fine-grained surface layers featuring effective surface seals are present.

The extended dry period between simulations 2.4 and 2.5 (120 hours) replicated the recovery of an ash bed after an initial period of sustained rainfall. After the dry period, both total and 300 s sub-period runoff rates reduced; total runoff for simulation 2.5 was 80% lower than that of simulation 2.4. Total runoff for simulation 2.5 fell to below the values produced during simulation 2.1 (Fig. 12), while apparent infiltration rates for simulation 2.5 were the lowest of all AB2 simulations. No bed-wide infiltration-excess overland flow occurred during the entire 1200-s duration period of simulation 2.5, a process that was visible after approximately 240 s of simulation 2.1 and during the entirety of simulations 2.2–2.4. This emphasises both the efficiency of surface sealing (of previously dry ash) throughout simulations 2.1–2.4, and the substantial increase in infiltration rates as a result of the 120-hour dry period before simulation 2.5. This is because

extended dry periods such as prior to simulation 2.5 impact the structure of surface seals (Assouline, 2004), with increased infiltration rates a product of reduced moisture content as well as inter-storm desiccation microcracking, producing a more granular seal structure that acts to increase the permeability of the ash bed (Kuhn and Bryan, 2004). The absence of ash pellets or easily remobilised surface particles immediately prior to simulation 2.5 prevents the filling of pores with tephra upon the commencement of rainfall and therefore surface sealing to the extent identified in simulations 2.1–2.4 could not take place within simulation 2.5.

4.3. *Simulation duration*

Changes in rainfall–runoff relationships during the course of individual simulations are intrinsically linked to both initial moisture content (and thus antecedent rainfall) and the total rainfall applied during the simulation. The rate of runoff increased during simulations for both AB1 and AB2, with this effect enhanced under low antecedent rainfall conditions (Fig. 10). Under low antecedent rainfall conditions, runoff rates increased gradually with time for both AB1 and AB2, caused by rising surface water content, and enhanced surface sealing induced by rain-beat compaction, respectively. As initial moisture content was increased through increased antecedent rainfall, runoff rates converged for all 300 s sub-periods, indicating more consistent runoff rates during the course of the simulations (Fig. 10).

4.4. *Implications for rain-triggered lahar research*

Using a new, inexpensive experimental set up, the present study has investigated and isolated some of the key factors previously identified in both field-based studies of RTLs and statistical analysis of RTL initiation thresholds. Antecedent impacts on lahar frequency have been highlighted previously at Soufrière Hills (Barclay et al., 2007), Tungurahua (Jones et al., 2015),

Merapi (Lavigne et al., 2000a), Yakedake (Okano et al., 2012), Colima (Capra et al., 2010) and Semeru (Lavigne and Suwa, 2004). The present study demonstrates that when residual ash moisture content is high, antecedent rainfall-driven runoff is increased and lag time is decreased, enhancing the potential for both lower intensity and shorter duration storm events to trigger lahars. This indicates that both lahar frequency and lahar volume can be expected to increase with heightened antecedent rainfall (e.g., as identified at Tungurahua by Jones et al., 2015). The impact of extended dry spells is also demonstrated, with a 120 hour-long dry spell reducing total runoff to below that produced by the initial dry ash bed but not affecting erosion rates. Wetting and drying cycles thus play an important role in surface seal development, destruction and potential re-development, highlighting the importance of the post-eruption rainfall and drying history upon rainfall–runoff relationships and thus lahar-triggering thresholds.

Surface sealing of fine-grained tephra has been reported to cause increased lahar frequencies at Unzen (Yamakoshi and Suwa, 2000) and Ruapehu (Manville et al., 2000), while coarse, permeable deposits have been reported to cause reduced lahar frequencies at Merapi (Lavigne et al., 2000a) and Mayon (Rodolfo and Arguden, 1991). The development of surface seals, as observed in AB2 simulations, may act to delay peak post-eruption RTL probability, as early rainfall that is insufficient to remobilise the ash may instead prime it for later major lahars by creating an effective surface seal. This study emphasises the compound impacts of both a fining of the grain-size distribution and increased antecedent rainfall, displaying a 1790% increase in runoff and a 92% decrease in lag time for an ash bed with a fine-grained surface layer that had received 102 mm of 72-hour antecedent rainfall relative to a coarse dry ash bed.

Primarily due to a limited ash supply, the present study focused on grain size distribution and antecedent rainfall as independent variables. However, a similar experimental configuration could be utilised to isolate and study the impact of factors including gradient, rainfall intensity, rainfall duration, vegetation coverage and deposit thickness on RTL generation under controlled

conditions. The extension of the length of the ash bed would also facilitate the further investigation of the role of rill formation in RTL initiation.

5. Conclusions

A new and repeatable rainfall simulation-based experimental configuration has been used to study conditions analogous to those present during the initiation of rain-triggered lahars. Calibrated rainfall simulations have illustrated that both finer-grained surface material and increased antecedent rainfall increase runoff rates and decrease runoff lag time from laboratory-constructed tephra beds. Surface sealing occurred within minutes of rainfall on dry fine-grained surface tephra after initial airborne remobilisation and ash pellet formation but was not evident on coarser material. This surface seal reduced infiltration rates and generated downslope sediment transport via entrainment within infiltration-excess overland flow, illustrating the potential for enhanced lahar initiation after initial surface seal-inducing rainfall. Additionally, an antecedent rainfall-driven increase in runoff and a reduction in runoff lag time highlights the potential for lahar formation from both lower intensity and shorter duration storm events when tephra residual moisture content is high. Conversely, extended dry periods reduced the effectiveness of the surface seal and increased infiltration rates, highlighting the importance of wetting and drying cycles upon lahar initiation thresholds. Rainsplash-driven particle detachment was the primary transport mechanism of sediment from simulations featuring coarser surface tephra due to consistently high infiltration rates, irrespective of antecedent rainfall. Rainfall simulations of the nature designed and developed in this study could be utilised to investigate a range of features related to lahar initiation under controlled conditions. Expanding the range of studied ash samples, rainfall parameters, antecedent conditions and slope angles would give further insight into lahar-triggering processes that are often difficult to directly examine in the field due to access issues associated with the location of lahar initiation zones.

Acknowledgements

We are thankful to STREVA (NERC/ESRC consortium NE/J02483X/1) for funding this study, and for NERC funding to the Sorby Environmental Fluid Dynamics Laboratory. Gareth Keevil, Kirk Handley and Bill Murphy are thanked for help with experimental design and setup. We also thank the editor, Dr. Oguchi, and an anonymous reviewer for their constructive comments on the manuscript.

References

Alexander, J., Barclay, J., Susnik, J., Loughlin, S.C., Herd, R.A., Darnell, A., Crosweller, S., 2010. Sediment-charged flash floods on Montserrat: The influence of synchronous tephra fall and varying extent of vegetation damage. Journal of Volcanology and Geothermal Research 194(4), 127-138. 10.1016/j.jvolgeores.2010.05.002.

Arboleda, R., Martinez, M., 1996. 1992 Lahars in the Pasig-Potrero River System. In: C. Newhall, R. Punongbayan (Eds.), Fire and Mud, Eruptions and Lahars of Mt Pinatubo, Philippines. PHIVOLCS/University of Washington Press, Quezon City/Seattle, pp. 1045-1055.

Arguden, A., Rodolfo, K., 1990. Sedimentologic and dynamic differences between hot and cold laharic debris flows of Mayon Volcano, Philippines. Geological Society of America Bulletin 102(7), 865-876. 10.1130/0016-7606(1990)102<0865:saddbh>2.3.co;2.

Assouline, S., 2004. Rainfall-induced soil surface sealing: A critical review of observations, conceptual models, and solutions. Vadose Zone Journal 3(2), 570-591. 10.2113/3.2.570.

Barclay, J., Alexander, J., Susnik, J., 2007. Rainfall-induced lahars in the Belham Valley, Montserrat, West Indies. Journal of the Geological Society 164(4), 815-827. 10.1144/0016-76492006-078.

Bernard, B., 2013. Homemade ashmeter: a low-cost, high-efficiency solution to improve tephra field-data collection for contemporary explosive eruptions. Journal of Applied Volcanology 2(1), 1-9. 10.1186/2191-5040-2-1.

Bradford, J.M., Ferris, J.E., Remley, P.A., 1987. Interrill soil erosion processes: I. Effect of surface sealing on infiltration, runoff, and soil splash detachment. Soil Science Society of America Journal 51(6), 1566-1571. 10.2136/sssaj1987.03615995005100060029x.

Brazier, S., Sparks, R.S.J., Carey, S.N., Sigurdsson, H., Westgate, J.A., 1983. Bimodal grain size distribution and secondary thickening in air-fall ash layers. Nature 301(5896), 115-119. 10.1038/301115a0.

Bryan, R.B., 2000. Soil erodibility and processes of water erosion on hillslope. Geomorphology 32(3-4), 385-415. 10.1016/s0169-555x(99)00105-1.

Capra, L., Borselli, L., Varley, N., Gavilanes-Ruiz, J.C., Norini, G., Sarocchi, D., Caballero, L., Cortes, A., 2010. Rainfall-triggered lahars at Volcán de Colima, Mexico: Surface hydro-repellency as initiation process. Journal of Volcanology and Geothermal Research 189(1-2), 105-117. 10.1016/j.jvolgeores.2009.10.014.

Castillo, V.M., Gómez-Plaza, A., Martínez-Mena, M., 2003. The role of antecedent soil water content in the runoff response of semiarid catchments: a simulation approach. Journal of Hydrology 284(1–4), 114-130. 10.1016/S0022-1694(03)00264-6.

Cerda, A., Doerr, S.H., 2008. The effect of ash and needle cover on surface runoff and erosion in the immediate post-fire period. CATENA 74(3), 256-263. 10.1016/j.catena.2008.03.010.

Christiansen, J., 1942. Irrigation by sprinkling University of California Agricultural Experimental Station Bulletin 670, 110-116.

Davila, N., Capra, L., Gavilanes-Ruiz, J.C., Varley, N., Norini, G., Vazquez, A.G., 2007. Recent lahars at Volcán de Colima (Mexico): Drainage variation and spectral classification. Journal of Volcanology and Geothermal Research 165(3-4), 127-141. 10.1016/j.jvolgeores.2007.05.016.

de Bélizal, E., Lavigne, F., Hadmoko, D.S., Degeai, J.-P., Dipayana, G.A., Mutaqin, B.W., Marfai, M.A., Coquet, M., Mauff, B.L., Robin, A.-K., Vidal, C., Cholik, N., Aisyah, N., 2013. Rain-triggered lahars following the 2010 eruption of Merapi volcano, Indonesia: A major risk. Journal of Volcanology and Geothermal Research 261, 330-347. 10.1016/j.jvolgeores.2013.01.010.

Dibyosaputro, S., Dipayana, G., Nugraha, H., Pratiwi, K., Valeda, H., 2015. Lahar at Kali Konto after the 2014 Eruption of Kelud Volcano, East Java: Impacts and Risk. Forum Geografi 29(1), 59-72.

Doyle, E.E., Cronin, S.J., Cole, S.E., Thouret, J.C., 2010. The coalescence and organization of lahars at Semeru volcano, Indonesia. Bulletin of Volcanology 72(8), 961-970. 10.1007/s00445-010-0381-8.

Dumaisnil, C., Thouret, J.C., Chambon, G., Doyle, E.E., Cronin, S.J., Surono, 2010. Hydraulic, physical and rheological characteristics of rain-triggered lahars at Semeru volcano, Indonesia. Earth Surface Processes and Landforms 35(13), 1573-1590. 10.1002/Esp.2003.

Dunne, T., Zhang, W., Aubry, B.F., 1991. Effects of rainfall, vegetation, and microtopography on infiltration and runoff. Water Resources Research 27(9), 2271-2285. 10.1029/91WR01585.

Gilley, J.E., Elliot, W.J., Laflen, J.M., Simanton, J.R., 1993. Critical shear stress and critical flow rates for initiation of rilling. Journal of Hydrology 142(1), 251-271. 10.1016/0022-1694(93)90013-Y.

Gómez, J.A., Darboux, F., Nearing, M.A., 2003. Development and evolution of rill networks under simulated rainfall. Water Resources Research 39(6). 10.1029/2002wr001437.

Gran, K.B., Montgomery, D.R., 2005. Spatial and temporal patterns in fluvial recovery following volcanic eruptions: Channel response to basin-wide sediment loading at Mount Pinatubo, Philippines. Geological Society of America Bulletin 117(1-2), 195-211. 10.1130/B25528.1.

Gudmundsson, M.T., Thordarson, T., Hoskuldsson, A., Larsen, G., Bjornsson, H., Prata, F.J., Oddsson, B., Magnusson, E., Hognadottir, T., Petersen, G.N., Hayward, C.L., Stevenson, J.A., Jonsdottir, I., 2012. Ash generation and distribution from the April-May 2010 eruption of Eyjafjallajokull, Iceland. Scientific Reports 2, 1-12. 10.1038/srep00572.

Hawkins, R.H., Cundy, T.W., 1987. Steady-state analysis of infiltration and overland flow for spatially-varied hillslopes. Journal of the American Water Resources Association 23(2), 251-256. 10.1111/j.1752-1688.1987.tb00804.x.

Hikida, M., Moriyama, M., Nagai, Y., 2007. Warning system for debris flow hazards at Sakurajima Volcano, Japan. In: C.L. Chen, J.J. Major (Eds.), Debris-Flow Hazards Mitigation: Mechanics, Prediction, and Assessment. Millpress Science Publishers, Rotterdam, pp. 593-602.

Hodgson, K.A., Manville, V.R., 1999. Sedimentology and flow behavior of a rain-triggered lahar, Mangatoetoenui Stream, Ruapehu volcano, New Zealand. Geological Society of America Bulletin 111(5), 743-754. 10.1130/0016-7606(1999)111<0743:safboa>2.3.co;2.

Horton, R.E., 1933. The role of infiltration in the hydrologic cycle. Transactions, American Geophysical Union 14(1), 446-460. 10.1029/TR014i001p00446.

Huang, J., Wu, P., Zhao, X., 2013. Effects of rainfall intensity, underlying surface and slope gradient on soil infiltration under simulated rainfall experiments. CATENA 104, 93-102. 10.1016/j.catena.2012.10.013.

Janda, R., Daag, A., Delos Reyes, P., Newhall, C., Pierson, T., Punongbayan, R., Rodolfo, K., Solidum, R., Umbal, J., 1996. Assessment and response to lahar hazard around Mt Pinatubo, 1991 to 1993. In: C. Newhall, R. Punongbayan (Eds.), Fire and Mud, Eruptions and Lahars of Mt Pinatubo, Philippines. PHIVOLCS/University of Washington Press, Quezon City/Seattle, pp. 107-140.

Jenkins, S.F., Phillips, J.C., Price, R., Feloy, K., Baxter, P.J., Hadmoko, D.S., de Bélizal, E., 2015. Developing building-damage scales for lahars: application to Merapi volcano, Indonesia. Bulletin of Volcanology 77(9), 10.1007/s00445-00015-00961-00448.

Jensen, E.H., Helgason, J.K., Einarsson, S., Sverrisdottir, G., Höskuldsson, A., Oddsson, B., 2013. Lahar, floods and debris Flows resulting from the 2010 eruption of Eyjafjallajökull: observations, mapping, and modelling. In: C. Margottini, P. Canuti, K. Sassa (Eds.), Landslide Science and Practice: Volume 3: Spatial Analysis and Modelling. Springer Berlin, pp. 435-440.

Jomaa, S., Barry, D.A., Heng, B.C.P., Brovelli, A., Sander, G.C., Parlange, J.Y., 2013. Effect of antecedent conditions and fixed rock fragment coverage on soil erosion dynamics through multiple rainfall events. Journal of Hydrology 484, 115-127. 10.1016/j.jhydrol.2013.01.021.

Jones, R., Manville, V., Andrade, D., 2015. Probabilistic analysis of rain-triggered lahar initiation at Tungurahua volcano. Bulletin of Volcanology 77(8). 10.1007/s00445-015-0946-7.

Kuhn, N.J., Bryan, R.B., 2004. Drying, soil surface condition and interrill erosion on two Ontario soils. CATENA 57(2), 113-133. 10.1016/j.catena.2003.11.001.

Larsen, M.C., Simon, A., 1993. A rainfall intensity-duration threshold for landslides in a humid-tropical environment, Puerto Rico. Geografiska Annaler. Series A, Physical Geography 75, 13-23. 10.2307/521049.

Lavigne, F., Thouret, J.C., 2003. Sediment transportation and deposition by rain-triggered lahars at Merapi Volcano, Central Java, Indonesia. Geomorphology 49(1-2), 45-69. 10.1016/s0169-555x(02)00160-5.

Lavigne, F., Suwa, H., 2004. Contrasts between debris flows, hyperconcentrated flows and stream flows at a channel of Mount Semeru, East Java, Indonesia. Geomorphology 61(1-2), 41-58. 10.1016/j.geomorph.2003.11.005.

Lavigne, F., Thouret, J.C., Voight, B., Suwa, H., Sumaryono, A., 2000a. Lahars at Merapi volcano, Central Java: an overview. Journal of Volcanology and Geothermal Research 100(1-4), 423-456. 10.1016/S0377-0273(00)00150-5.

Lavigne, F., Thouret, J.C., Voight, B., Young, K., LaHusen, R., Marso, J., Suwa, H., Sumaryono, A., Sayudi, D.S., Dejean, M., 2000b. Instrumental lahar monitoring at Merapi Volcano, Central Java, Indonesia. Journal of Volcanology and Geothermal Research 100(1-4), 457-478. 10.1016/S0377-0273(00)00151-7.

Le Bissonnais, Y., Renaux, B., Delouche, H., 1995. Interactions between soil properties and moisture content in crust formation, runoff and interrill erosion from tilled loess soils. CATENA 25(1), 33-46. 10.1016/0341-8162(94)00040-L.

Leavesley, G., Lusby, G., Lichty, R., 1989. Infiltration and erosion characteristics of selected tephra deposits from the 1980 eruption of Mt St Helens, Washington, USA. Hydrological Sciences 34(3), 339-353.

Liu, H., Lei, T.W., Zhao, J., Yuan, C.P., Fan, Y.T., Qu, L.Q., 2011. Effects of rainfall intensity and antecedent soil water content on soil infiltrability under rainfall conditions using the run off-on-out method. Journal of Hydrology 396(1-2), 24-32. 10.1016/j.jhydrol.2010.10.028.

Loch, R.J., Robotham, B.G., Zeller, L., Masterman, N., Orange, D.N., Bridge, B.J., Sheridan, G., Bourke, J.J., 2001. A multi-purpose rainfall simulator for field infiltration and erosion studies. Australian Journal of Soil Research 39(3), 599-610. 10.1071/Sr00039.

Luk, S.-H., 1985. Effect of antecedent soil moisture content on rainwash erosion. *CATENA*, **12**(2-3), 129-139. 10.1016/0341-8162(85)90005-0.

Major, J.J., Mark, L.E., 2006. Peak flow responses to landscape disturbances caused by the cataclysmic 1980 eruption of Mount St. Helens, Washington. Geological Society of America Bulletin 118(7-8), 938-958. 10.1130/b25914.1.

Major, J.J., Yamakoshi, T., 2005. Decadal-scale change of infiltration characteristics of a tephra-mantled hillslope at Mount St Helens, Washington. Hydrological Processes 19(18), 3621-3630. 10.1002/Hyp.5863.Major, J.J., Pierson, T.C., Dinehart, R.L., Costa, J.E., 2000. Sediment yield following severe volcanic disturbance - A two-decade perspective from Mount St. Helens. Geology 28(9), 819-822. 10.1130/0091-7613(2000)28<819:Syfsvd>2.0.Co;2.

Major, J.J., Bertin, D., Pierson, T.C., Amigo, Á., Iroumé, A., Ulloa, H., Castro, J., 2016. Extraordinary sediment delivery and rapid geomorphic response following the 2008-2009 eruption of Chaitén Volcano, Chile. Water Resources Research 52(7), 5075-5094. 10.1002/2015wr018250.

Manville, V., Hodgson, K., Houghton, B., Keys, J., White, J., 2000. Tephra, snow and water: complex sedimentary responses at an active snow-capped stratovolcano, Ruapehu, New Zealand. Bulletin of Volcanology 62(4-5), 278-293. 10.1007/s004450000096.

Manville, V., Segschneider, B., Newton, E., White, J.D.L., Houghton, B.F., Wilson, C.J.N., 2009. Environmental impact of the 1.8 ka Taupo eruption, New Zealand: Landscape responses to a large-scale explosive rhyolite eruption. Sedimentary Geology 220(3-4), 318-336. 10.1016/j.sedgeo.2009.04.017.

Martinez, M., Arboleda, R., Delos Reyes, P., Gabinete, E., Dolan, M., 1996. Observations of 1992 Lahars along the Sacobia-Bamban River System. In: C. Newhall, R. Punongbayan (Eds.), Fire

and Mud, Eruptions and Lahars of Mt Pinatubo, Philippines. PHIVOLCS/University of Washington Press, Quezon City/Seattle, pp. 1033-1045.

Morgan, R., McIntyre, K., Vickers, A., Quinton, J., Rickson, R., 1997. A rainfall simulation study of soil erosion on rangeland in Swaziland. Soil Technology 11(3), 291-299. 10.1016/S0933-3630(97)00013-5.

Nammah, H., Larsen, F.E., McCool, D.K., Fritts, R., Molnau, M., 1986. Mt. St. Helens volcanic ash: Effect of incorporated and unincorporated ash of two particle sizes on runoff and erosion. Agriculture, Ecosystems & Environment 15(1), 63-72. 10.1016/0167-8809(86)90114-3.

Nearing, M.A., Foster, G.R., Lane, L.J., Finkner, S.C., 1989. A process-based soil erosion model for USDA-Water Erosion Prediction Project technology. Transactions of the American Society of Agricultural Engineers 32(5), 1587-1593. 10.13031/2013.31195.

Ogawa, Y., Daimaru, H., Shimizu, A., 2007. Experimental study of post-eruption overland flow and sediment load from slopes overlain by pyroclastic-flow deposits, Unzen volcano, Japan. Géomorphologie : Relief, Processus, Environnement 13(3), 237-246. 10.4000/geomorphologie.3962.

Okano, K., Suwa, H., Kanno, T., 2012. Characterization of debris flows by rainstorm condition at a torrent on the Mount Yakedake volcano, Japan. Geomorphology 136(1), 88-94. 10.1016/j.geomorph.2011.04.006.

Orense, R.P., Ikeda, M., 2007. Damage caused by typhoon-induced lahar flows from Mayon Volcano, Philippines. Soils and Foundations 47(6), 1123-1132. 10.3208/sandf.47.1123.

Paguican, E.M.R., Lagmay, A.M.F., Rodolfo, K.S., Rodolfo, R.S., Tengonciang, A.M.P., Lapus, M.R., Baliatan, E.G., Obille, E.C., 2009. Extreme rainfall-induced lahars and dike breaching, 30 November 2006, Mayon Volcano, Philippines. Bulletin of Volcanology 71(8), 845-857. 10.1007/s00445-009-0268-8.

Pierson, F.B., Robichaud, P.R., Moffet, C.A., Spaeth, K.E., Williams, C.J., Hardegree, S.P., Clark, P.E., 2008. Soil water repellency and infiltration in coarse-textured soils of burned and unburned sagebrush ecosystems. CATENA 74(2), 98-108. 10.1016/j.catena.2008.03.011.

Pierson, T.C., 1985. Initiation and flow behavior of the 1980 Pine Creek and Muddy River Lahars, Mount-St-Helens, Washington. Geological Society of America Bulletin 96(8), 1056-1069. 10.1130/0016-7606(1985)96<1056:Iafbot>2.0.Co;2.

Pierson, T.C., Major, J.J., 2014. Hydrogeomorphic effects of explosive volcanic eruptions on drainage basins. Annual Review of Earth and Planetary Sciences 42(1), 469-507. 10.1146/annurev-earth-060313-054913.

Pierson, T.C., Major, J.J., Amigo, A., Moreno, H., 2013. Acute sedimentation response to rainfall following the explosive phase of the 2008-2009 eruption of Chaiten volcano, Chile. Bulletin of Volcanology 75(5), 1-17. 10.1007/S00445-013-0723-4.

Rodolfo, K., Arguden, A., 1991. Rain-lahar generation and sediment-delivery systems at Mayon Volcano, Philippines. In: R. Fisher, G. Smith (Eds.), Sedimentation in Volcanic Settings. SEPM, Special Publication 45, pp. 71-87.

Rodolfo, K., Umbal, J., Alonso, R., Remotigue, C., Paladio-Melosantos, L., Salvador, J., Evangelista, D., Miller, Y., 1996. Two years of lahars on the Western flank of mount Pinatubo: Initiation, flow processes, deposits, and attendant geomorphic and hydraulic changes. In: C. Newhall, R. Punongbayan (Eds.), Fire and Mud, Eruptions and Lahars of Mt Pinatubo, Philippines. PHIVOLCS/University of Washington Press, Quezon City/Seattle, pp. 989-1015.

Römkens, M.J.M., Helming, K., Prasad, S.N., 2002. Soil erosion under different rainfall intensities, surface roughness, and soil water regimes. CATENA 46(2-3), 103-123. 10.1016/s0341-8162(01)00161-8.

Scott, K., Janda, R., De La Cruz, E., Gabinete, E., Eto, I., Isada, M., Sexon, M., Hadley, K., 1996. Channel and sedimentation responses to large volumes of 1991 volcanic deposits on the East flank of Mt Pinatubo. In: C. Newhall, R. Punongbayan (Eds.), Fire and Mud, Eruptions

and Lahars of Mt Pinatubo, Philippines. PHIVOLCS/University of Washington Press, Quezon City/Seattle, pp. 971-989.

Segerstrom, K., 1950. Erosion studies at Paricutin, State of Michoacan, Mexico. USGS Bulletin 965-A, 164 pp.

Singh, S., Tack, F., Gabriels, D., Verloo, M., 2000. Heavy metal transport from dredged sediment derived surface soils in a laboratory rainfall simulation experiment. Water Air and Soil Pollution 118(1-2), 73-86. 10.1023/A:1005140726372.

Slattery, M.C., Bryan, R.B., 1992. Laboratory experiments on surface seal development and its effect on interrill erosion processes. Journal of Soil Science 43(3), 517-529. 10.1111/j.1365-2389.1992.tb00157.x.

Spence, R.J.S., Kelman, I., Baxter, P.J., Zuccaro, G., Petrazzuoli, S., 2005. Residential building and occupant vulnerability to tephra fall. Natural Hazards and Earth System Science 5(4), 477-494. 10.5194/nhess-5-477-2005.

Stinton, A.J., Cole, P.D., Stewart, R.C., Odbert, H.M., Smith, P., 2014. The 11 February 2010 partial dome collapse at Soufriere Hills Volcano, Montserrat. In: Wadge, G., Robertson, R.E.A., Voight, B., (Eds.), The eruption of Soufrière Hills Volcano, Montserrat from 2000 to 2010, Geological Society, London, Memoirs, 39(1), 133-152. 10.1144/m39.7.

Swanson, F.J., Jones, J.A., Crisafulli, C.M., Lara, A., 2013. Effects of volcanic and hydrologic processes on forest vegetation: Chaiten Volcano, Chile. Andean Geology 40(2), 359-391. 10.5027/andgeoV40n2-a10.

Thouret, J.C., Oehler, J.F., Gupta, A., Solikhin, A., Procter, J.N., 2014. Erosion and aggradation on persistently active volcanoes-a case study from Semeru Volcano, Indonesia. Bulletin of Volcanology 76(10). 10.1007/S00445-014-0857-Z.

Tisdall, A., 1951. Antecedent soil moisture and its relation to infiltration. Australian Journal of Agricultural Research 2(3), 342-348. 10.1071/AR9510342.

Tungol, N., Regalado, T., 1996. Rainfall, acoustic flow monitor records, and observed lahars of the Sacobia River in 1992. In: C. Newhall, R. Punongbayan (Eds.), Fire and Mud, Eruptions and Lahars of Mt Pinatubo, Philippines. PHIVOLCS/University of Washington Press, Quezon City/Seattle, pp. 1023-1033.

Umazano, A.M., Melchor, R.N., Bedatou, E., Bellosi, E.S., Krause, J.M., 2014. Fluvial response to sudden input of pyroclastic sediments during the 2008–2009 eruption of the Chaitén Volcano (Chile): The role of logjams. Journal of South American Earth Sciences 54, 140-157. 10.1016/j.jsames.2014.04.007.

Van Westen, C., Daag, A., 2005. Analysing the relation between rainfall characteristics and lahar activity at Mt Pinatubo, Philippines. Earth Surface Processes and Landforms 30, 1663-1674.

Waldron, H., 1967. Debris Flow and Erosion Control problems caused by the Ash eruptions of Irazu. USGS Bulletin 1241-1, 37 pp.

Wang, L., Shi, Z.H., Wang, J., Fang, N.F., Wu, G.L., Zhang, H.Y., 2014. Rainfall kinetic energy controlling erosion processes and sediment sorting on steep hillslopes: A case study of clay loam soil from the Loess Plateau, China. Journal of Hydrology 512, 168-176. 10.1016/j.jhydrol.2014.02.066.

Woods, S.W., Balfour, V.N., 2010. The effects of soil texture and ash thickness on the post-fire hydrological response from ash-covered soils. Journal of Hydrology 393(3-4), 274-286. 10.1016/j.jhydrol.2010.08.025.

Yamakoshi, T., Suwa, H., 2000. Post-eruption characteristics of surface runoff and sediment discharge on the slopes of pyroclastic-flow deposits, Mt Unzen, Japan. Transactions, Japanese Geomorphological Union 21, 469-497.

Yu, B., Rose, C.W., Coughlan, K.J., Fentie, B., 1997. Plot-Scale rainfall-runoff characteristics and modeling at six sites in Australia and Southeast Asia. Transactions of the American Society of Agricultural Engineers 40(5), 1295-1303. 10.13031/2013.21387.

Zhao, N., Yu, F., Li, C., Wang, H., Liu, J., Mu, W., 2014. Investigation of rainfall-runoff processes and soil moisture dynamics in grassland plots under simulated rainfall conditions. Water 6(9), 2671-2689. 10.3390/w6092671.

Figure and Table Captions

Fig. 1. Photographs illustrating erosion mechanisms of pyroclastic deposits. A) Rill network and channel development on the upper edifice of Calbuco Volcano, Chile (April 2015). B) Shallow landsliding of the tephra blanket in the Mangatoetoenui catchment of Ruapehu, New Zealand (October 1995). The 0.20 m-thick tephra layer was sliding on a thin (sub-cm) layer of fine-grained phreatomagmatic ash that was frozen to the underlying snow and ice.

Fig. 2. Schematic diagram illustrating the important factors in RTL initiation. A) Eruption deposits and impacts within proximal catchments. B) Post-eruption volcano-hydrologic processes within eruption-impacted catchments.

Fig. 3. Grain size distributions of Kelud and Chaitén ash samples as measured using a Malvern Mastersizer 2000E laser diffractometer.

Fig. 4. Schematic illustration of the complete experimental configuration utilised in this study.

Fig. 5. Spatial distribution of simulated rainfall using selected settings. A: Entire 1 m^2 rainfall calibration area. B: Optimal 0.3 m × 0.3 m sub-plot used for subsequent rainfall simulation experiments.

Fig. 6. Oblique views of contrasting initial ash bed responses to simulated rainfall Images are captured by camera 3 (Fig. 4) located adjacent to the downslope edge of the ash bed using a wide angled lens. The upslope extent of the ash bed is visible at the top of each image and the runoff hopper-protecting rain shield at the downslope extent of the ash bed is visible at the bottom right. A–C) Simulation 1.1 (AB1). D-I) Simulation 2.1 (AB2)

Fig. 7. Time series of total runoff during all rainfall simulations. A) AB1 (coarse ash) B) AB2 (coarse ash with fine ash surface layer). Note differences in vertical scale.

Fig. 8. Percentage increase of both total and 300 s sub-period runoff relative to the runoff generated during the initial rainfall simulations (simulations 1.1 and 2.1, respectively) of A) AB1 (coarse ash) and B) AB2 (coarse ash with fine ash surface layer) simulations as antecedent rainfall was increased. Best fit least-squares linear regression lines are displayed for simulations 1.1 and 2.1.

Fig. 9. Total runoff mass at the conclusion of 1200 s duration rainfall simulations for AB1 (coarse ash) and AB2 (coarse ash with fine surface layer) under variable antecedent rainfall conditions. Best fit least-squares linear regression lines are displayed for both AB1 and AB2.

Fig. 10. Runoff rates for the four 300 s sub-periods of both AB1 (coarse ash) and AB2 (coarse ash with fine ash surface layer) during rainfall simulations featuring variable antecedent conditions. Best fit least-squares linear regression lines are displayed for each 300 s sub-period of both AB1 and AB2.

Fig. 11. Runoff lag times of AB1 (coarse ash) and AB2 (coarse ash with fine ash surface layer) under variable antecedent conditions. Best fit least-squares linear regression lines are displayed for both AB1 and AB2.

Fig. 12. Apparent infiltration rate (f') curves for all AB1 and AB2 rainfall simulations derived from rainfall and runoff rate information. Best fit least-squares linear regression lines are displayed for AB1 simulations, and least-squares power regression lines are displayed for AB2 simulations.

Table 1. Grain size distribution characteristics of Kelud and Chaitén ash samples as measured using a Malvern Mastersizer 2000E laser diffractometer.

Table 2. Antecedent rainfall amounts (in mm) applied to the tephra beds at timescales ranging from 24 hours to 192 hours prior to the commencement of each rainfall simulation.

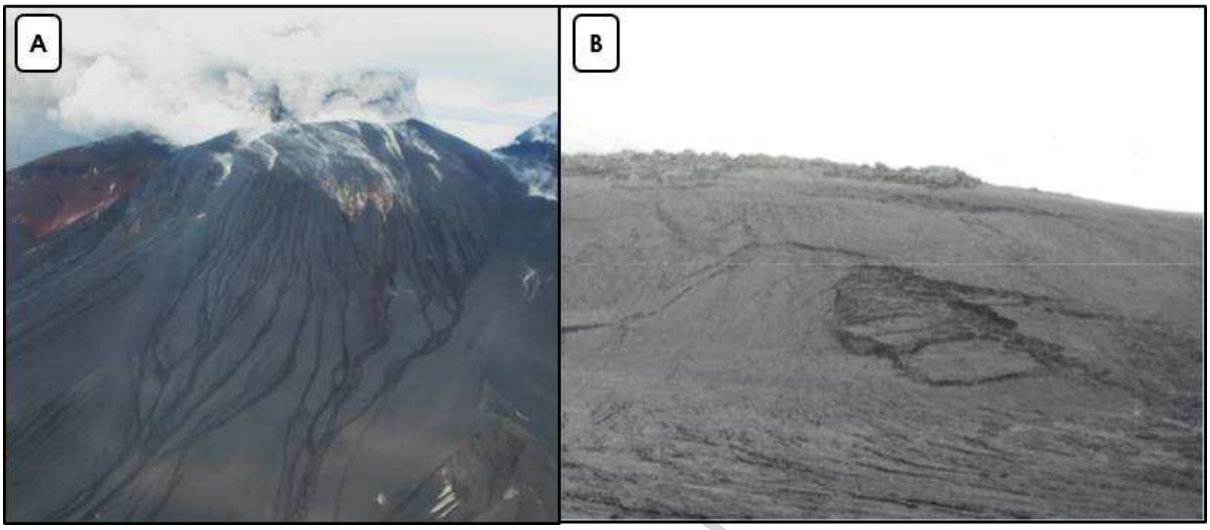

Figure 1

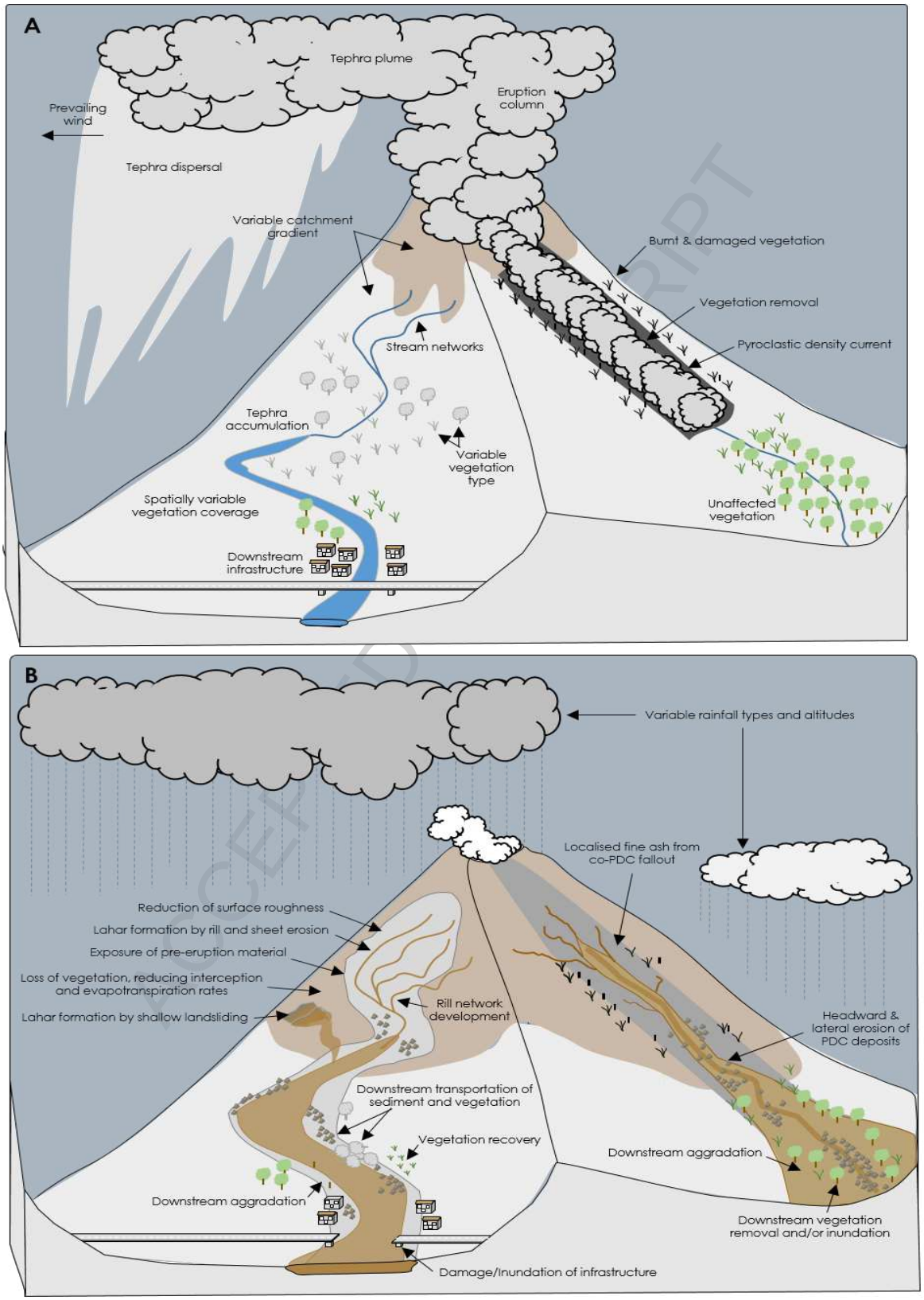

Figure 2

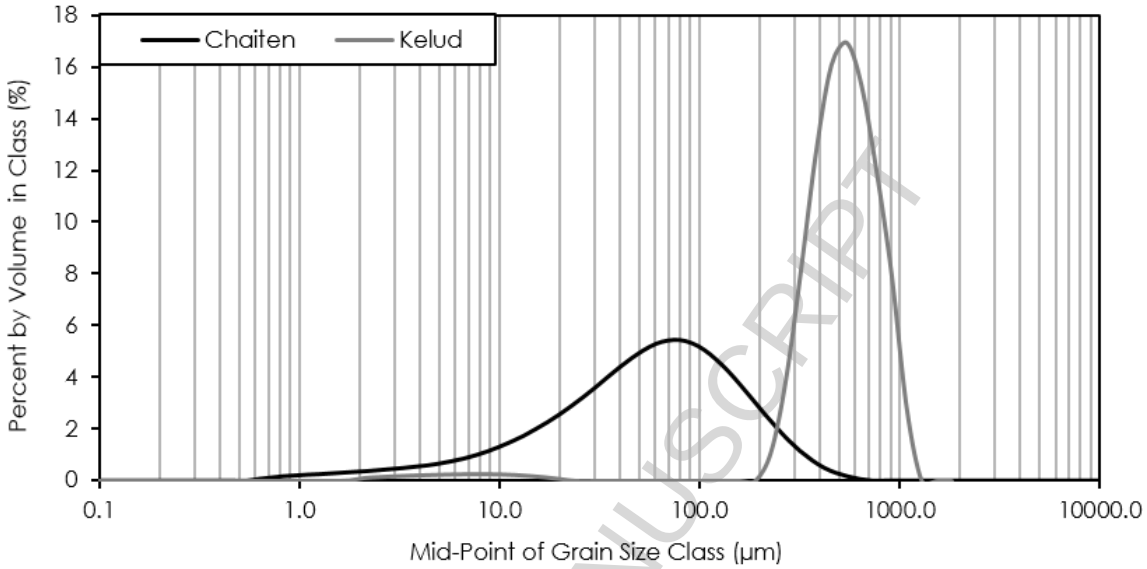

Figure 3

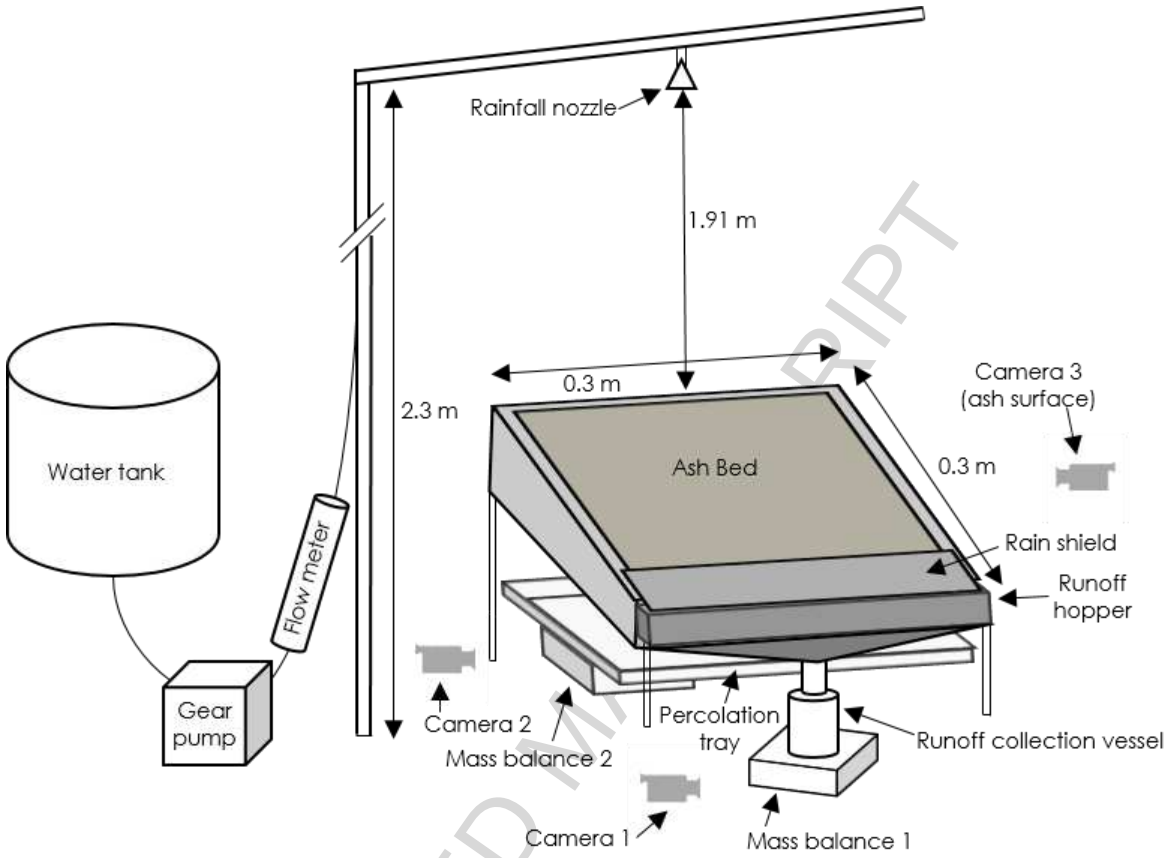

Figure 4

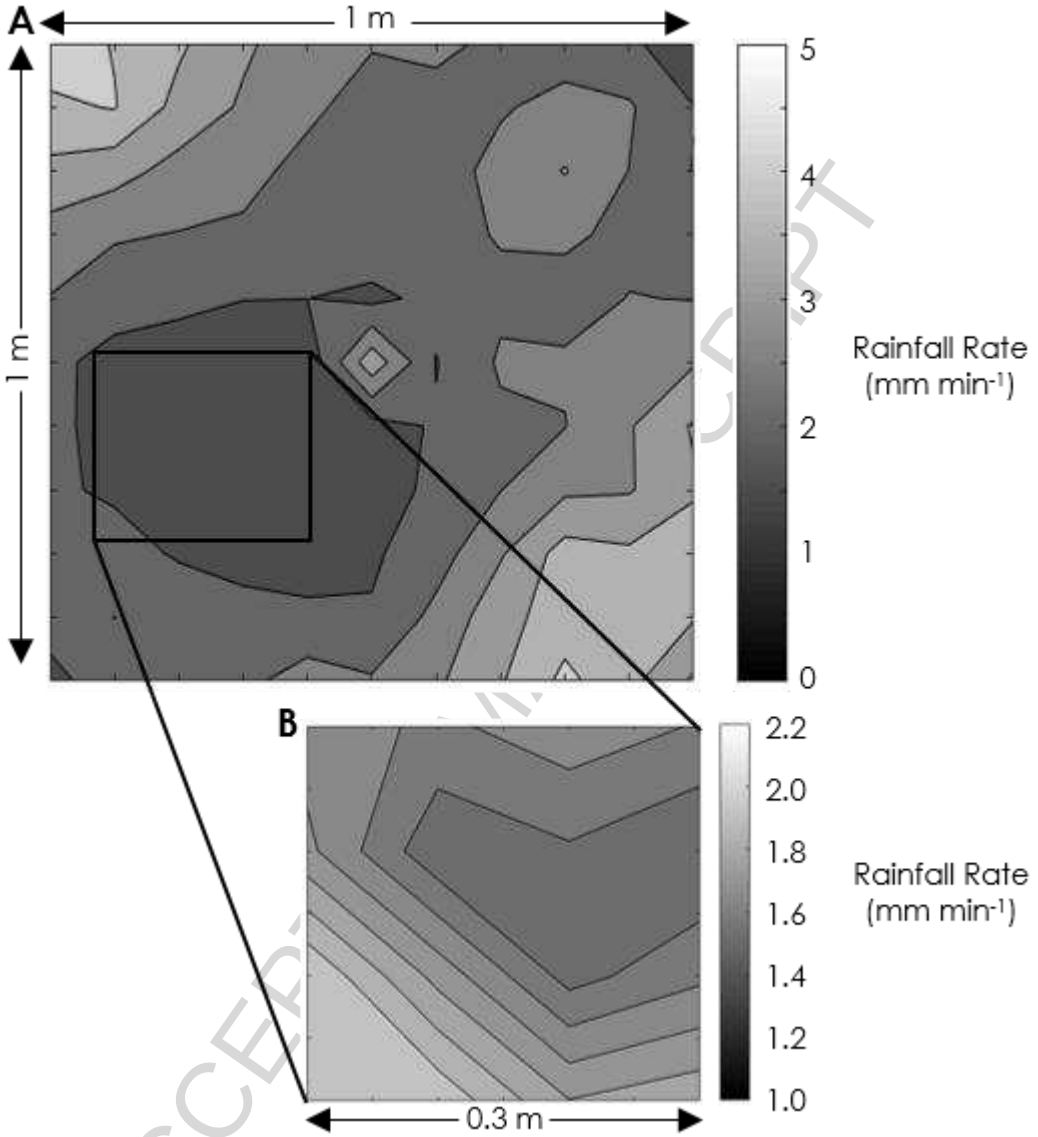

Figure 5

Figure 6

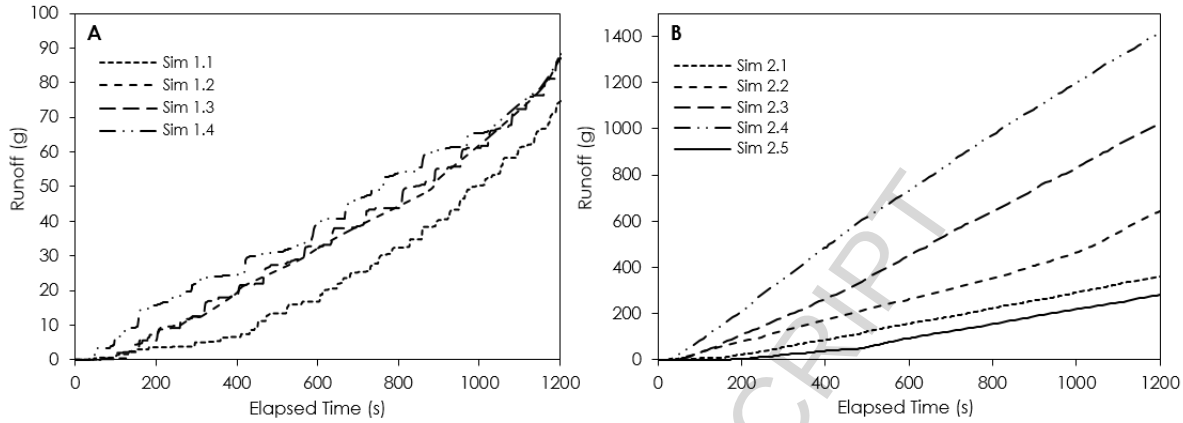

Figure 7

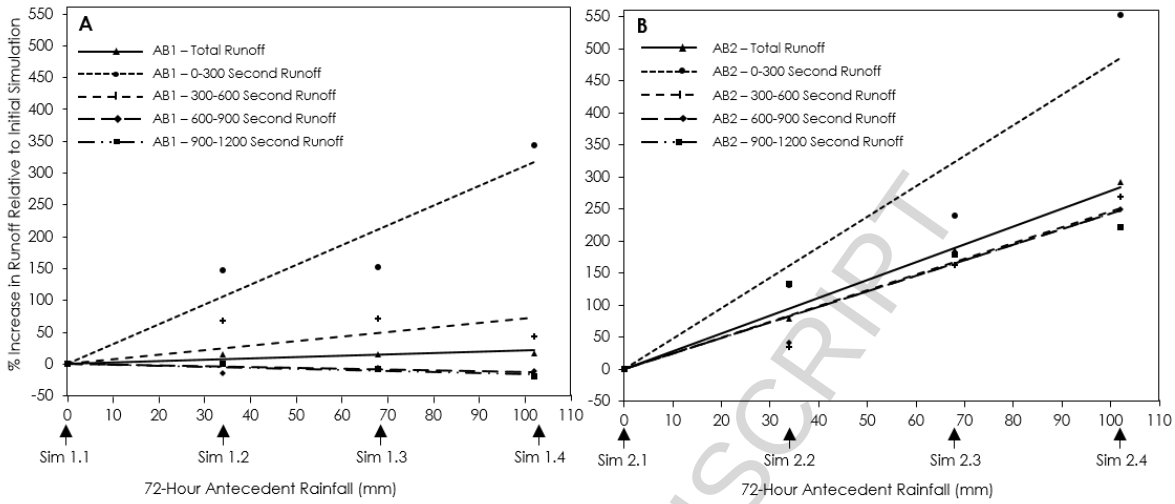

Figure 8

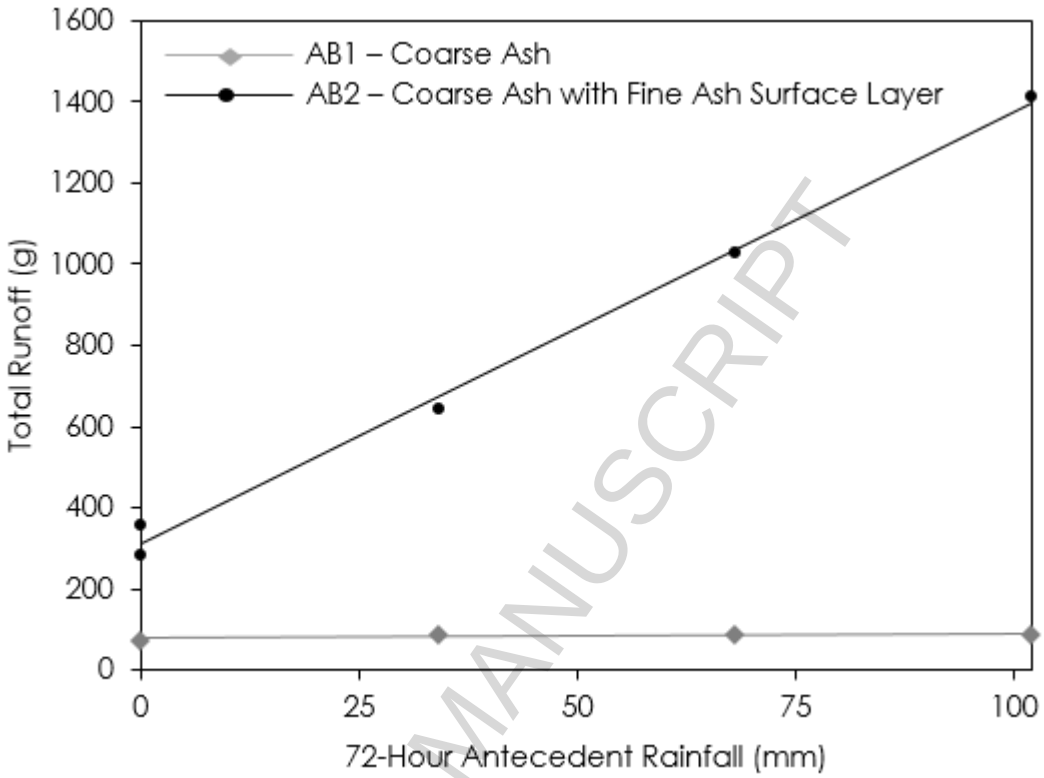

Figure 9

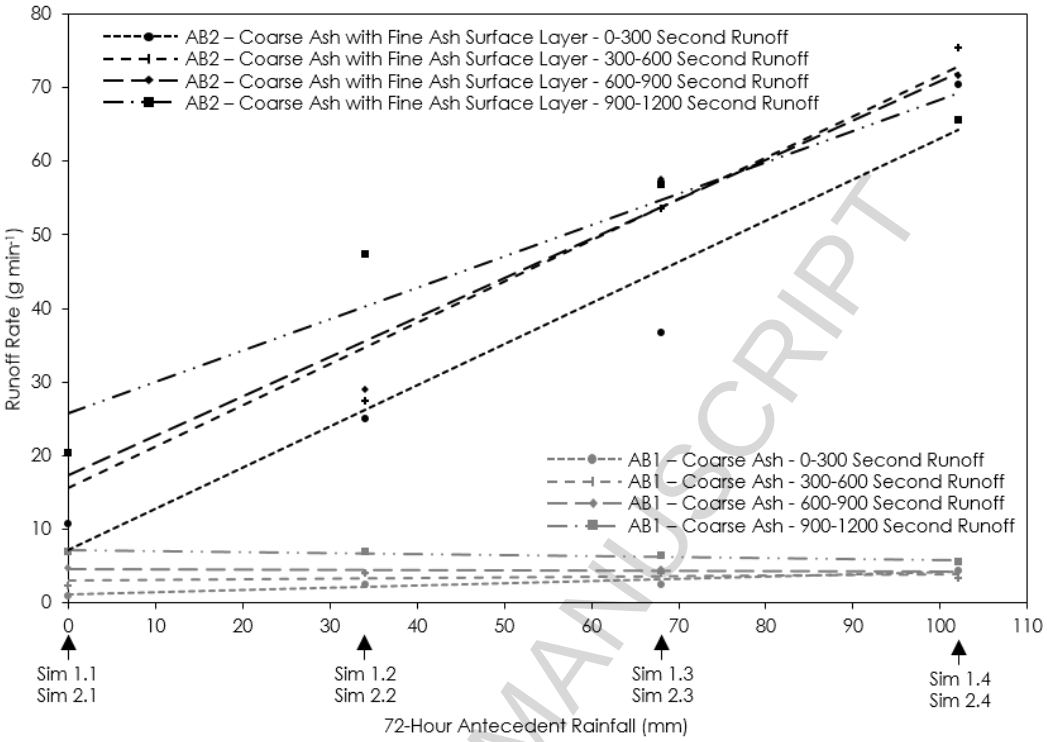

Figure 10

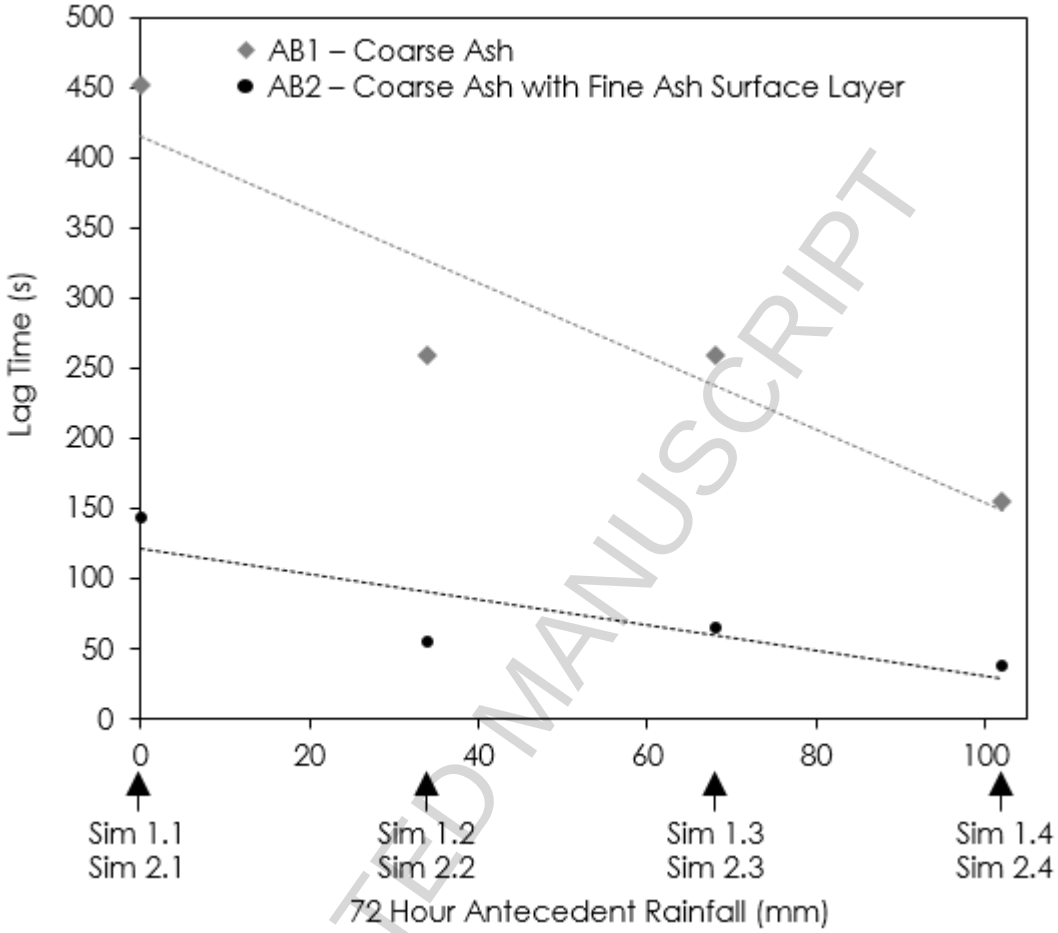

Figure 11

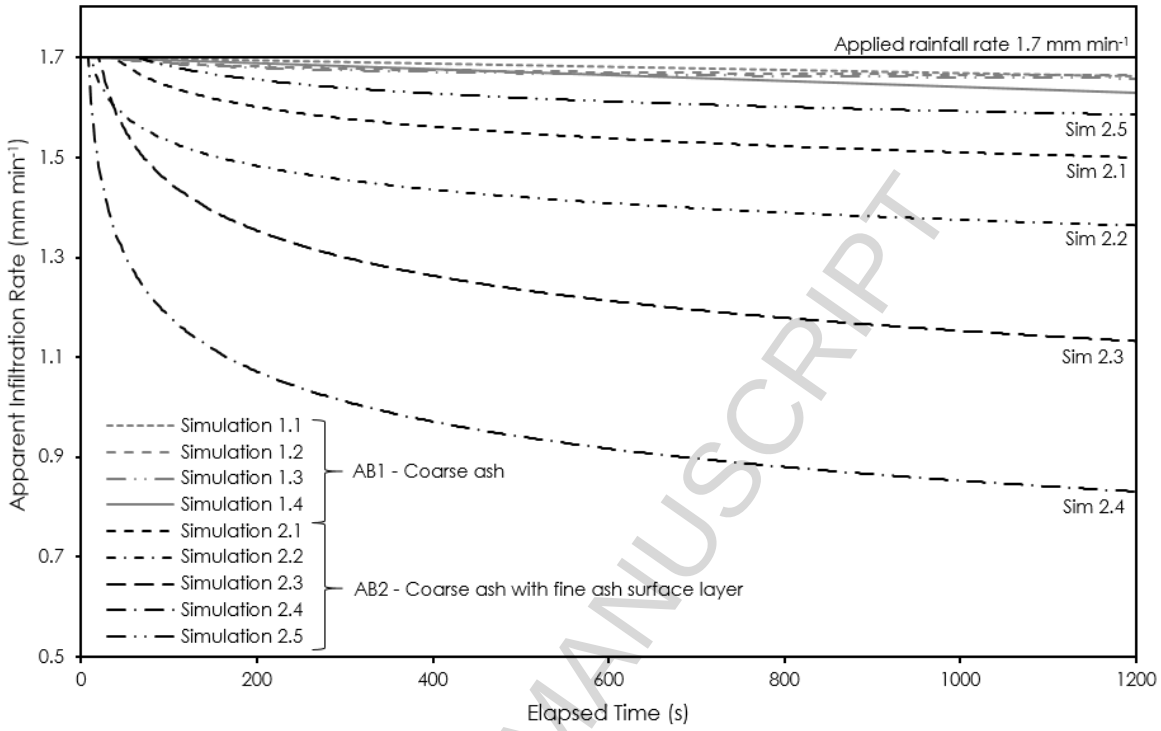

Figure 12

Table 1

	d_{10}	d_{20}	d_{50}	d_{80}	d_{90}
Chaitén (µm)	9.4	19.2	54.3	120.5	173.9
Kelud (µm)	313.8	374.7	525.8	732.5	852.2

Table 2

Simulation:	1.1	1.2	1.3	1.4	2.1	2.2	2.3	2.4	2.5
Antecedent Rainfall - 24 HR - (mm):	0	34	34	34	0	34	34	34	0
Antecedent Rainfall - 48 HR - (mm):	0	34	68	68	0	34	68	68	0
Antecedent Rainfall - 72 HR - (mm):	0	34	68	102	0	34	68	102	0
Antecedent Rainfall - 96 HR - (mm):	0	34	68	102	0	34	68	102	0
Antecedent Rainfall - 120 HR - (mm):	0	34	68	102	0	34	68	102	0
Antecedent Rainfall - 144 HR - (mm):	0	34	68	102	0	34	68	102	34
Antecedent Rainfall - 168 HR - (mm):	0	34	68	102	0	34	68	102	68
Antecedent Rainfall - 192 HR - (mm):	0	34	68	102	0	34	68	102	102

Highlights

- Analogous rain-triggered lahar source conditions examined using simulated rainfall
- Increased antecedent rainfall heightened runoff rates and reduced runoff lag times
- Fine-grained surface tephra layers formed runoff enhancing surface seals
- Extended dry periods reduced surface seal effectiveness and enhanced infiltration